PHYSICAL REVIEW A VOLUME 24, NUMBER 4 OCTOBER 1981

Semiclassical theory of resonant three-wave parametric interactions: Second-harmonic generation

T. A. DeTemple, L. A. Bahler, and J. Osmundsen
Electro-Physics Laboratory, Department of Electrical Engineering, University of Illinois, Urbana, Illinois 61801
(Received 11 May 1981)

Motivated by recent experiments on second-harmonic generation in three-level systems [K. S. Yngvesson and E. L. Kollberg, Appl. Phys. Lett. 36, 104 (1980)], a semiclassical description of resonant three-wave parametric interactions in three nondegenerate levels is considered. Within the limitations of the rotating-wave approximation, analytical nonperturbative solutions for the nonlinear polarization are derived, which are then coupled to Maxwell's equations and integrated numerically. The results of sample calculations for second-harmonic generation show (a) a maximum harmonic conversion occurs on full resonance, (b) the conversion efficiency can be $> 50\%$ but requires a strongly saturating pump, (c) the conversion distance increases with pumping intensity, and (d) the inclusion of ac Stark splittings is crucial for the achievement of high conversion efficiency. The role of level splittings is further explored for the case of a resonant parametric oscillator.

I. INTRODUCTION

Optical second-harmonic generation, the first optical nonlinearity to be observed, is a standard multiplication technique used from the infrared to the ultraviolet.[1] Although usually discussed from the standpoint of a bulk nonlinear susceptibility, the process can be described in terms of a multiphoton parametric interaction, in which case the explicit matrix element and transition detuning dependences can be seen.[2,3] For the case of bulk nonlinearities in transparent media, the nonlinear coefficients are small because the detunings, in general, are very large. In contrast, there are some candidate systems for which the waves may be at or near resonance so that a resonant enhancement or increase in the nonlinear coefficient occurs. An example is seen in the studies on two-photon resonant, optical second- and third-harmonic generation in gases.[4,5]

In the case of optical second-harmonic generation, situations involving resonant enhancement have been noted in paramagnetic spin systems tuned by external magnetic fields. Kellington was the first to explore this effect in room-temperature ruby samples pumped at 9.4 GHz.[6] In subsequent studies on this system, the line shapes and interference effects due to thermally populated states were observed.[7-9] Very recently, Yngvesson and Kollberg have studied resonantly enhanced second-harmonic generation in iron-doped rutile pumped at 24 GHz.[10] The interesting aspects of their experiment are the observation of a conversion efficiency of 10^{-4} obtained at full resonance and the saturation achieved at a modest pumping power of ~10 mW. Closely related to these are a number of different observations of resonant difference frequency generation in ruby, most notably by Inaba and Hidaka,[11] and in chromium-doped rutile by Dathe *et al.*[12]

Unlike bulk second-harmonic generation for which full conversion is known to be possible under phase-matched conditions, there have been relatively few studies directed at the limits of second-harmonic generation under resonant conditions.[2,13] In a now-classic paper, Clogston initially addressed this problem from a maser standpoint but ultimately treated the case of a parametric oscillator with a strong pump but weak signal and idler fields.[14] From a multiphoton single-atom interaction treatment, Senitzky concluded that resonant sum-frequency generation and second-harmonic generation should be possible.[15] In apparent support of Kellington's observations, Andresen and co-workers derived the nonlinear susceptibility in a perturbation limit and showed the origin of the interference effect in terms of contributions from excited states.[7,16] Bloembergen and Shen considered this problem in general but ultimately solved Clogston's parametric case for a strong pump and weak signal and idler waves.[17] They also indicated some of the multitude of processes present near resonance by expressing their result in terms of one- and two-photon (Raman) interactions and a parametric interaction. Voskanyan *et al.* have considered the case of resonant second-harmonic generation and derived a correct parametric result valid for a strong pump but weak harmonic.[9] They did not consider the one- and two-photon processes which occur under the same conditions. Hänsch and Toschek treated parametric interactions from a perturbation standpoint and pointed out the multipole moment requirements for the observation of such effects in systems which possess a center of inversion.[18] There have been many other treatments of parametric interactions involving two input fields (difference frequency mixing) in the perturbation limit[11,19,20] and by Javan and Szöke in the

strong-pump but weak-signal-field limit.[21] The general treatment valid for arbitrary field intensities and including propagation effects has not been presented.

In this paper we address, theoretically, resonantly enhanced second-harmonic generation in three-level systems. Our motivation for this study is based on the remarkable observation by Yngvesson and Kollberg and on the lack of a complete treatment of this problem, including propagation. The treatment is naturally resolved into the determination of the relevant nonlinear polarizations due to the presence of all waves and to the coupling to and effect of these polarizations on the propagating fields. The treatment differs from others in the inclusion of propagation effects and in the lack of restrictions on the field intensities. In the next section, we outline the solutions for the nonlinear polarizations which are derived from a semiclassical density-matrix approach in a nonperturbative limit valid for near resonant tuning conditions. Section III addresses local solutions illustrating perturbative and selected nonperturbative limits of resonant second-harmonic generation. Section IV addresses propagation and the details of the limitations on the conversion which, in general, can be quite high, $>50\%$. This is followed by a synopsis of the paper and conclusions.

II. BASIC EQUATIONS

The linkage diagram appropriate to near resonant three-wave parametric interactions is shown in Fig. 1(a). What is ultimately desired for a description of these interactions is the specification of the nonlinear polarizations associated with each wave in terms of the relevant matrix elements, detunings, fields, and populations. Given these, the relative strengths of the interaction can be determined from a suitable field description based on Maxwell's equations. In what follows, we shall recast a density-matrix description of this system into a form from which partial analytical solutions will be derived. By this, we mean that the solutions will be comprised of products of coefficients and populations. The coefficients are obtained analytically but the populations are determined numerically except for selected limits. With these results, the relevant spectroscopy of the system can be studied algebraically but the conversion dynamics have to be considered numerically. The solutions will be discussed more fully in the next section for the specific case of second-harmonic generation for which $\vec{E}_1(\omega_1)=\vec{E}_2(\omega_2)$ and $\omega_3=2\omega_1$.

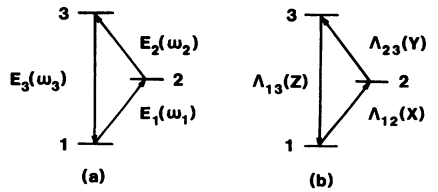

FIG. 1. (a) Linkage diagram for three-wave parametric interactions in a three-level system. (b) Equivalent linkage diagram in (a) expressed in terms of Rabi frequencies, Λ_{ij}, and detunings $X=\Omega_{21}-\omega_1$, $Y=\Omega_{32}-\omega_2$, and $Z=\Omega_{31}-\omega_3$ in the near resonant tuning case.

Shown in Fig. 2 is an illustration of the number of different processes which can exist under near resonant tuning conditions. The parametric gain will be seen later to share the same matrix elements and detunings as the two-photon absorption coefficient of the two waves creating the gain. The latter process is known to be a maximum on two-photon and one-photon resonance; that is, when the two waves are exactly on line center.[22] Under these conditions, the parametric gain is a maximum but the parametrically generated field is exactly on one-photon resonance and would experience a strong loss. To compensate for this, the pump fields may be increased causing two effects to ultimately occur: population saturation and level splittings. Both effects have been considered previously for the serial two-wave problem.[23-26] In particular, one strong saturating wave is known to split the two coupled states into a doublet, Autler-Townes splitting,[27] experimentally observed,[28,29] whereas two strong waves will split the three coupled states into a triplet.[23,24,30]

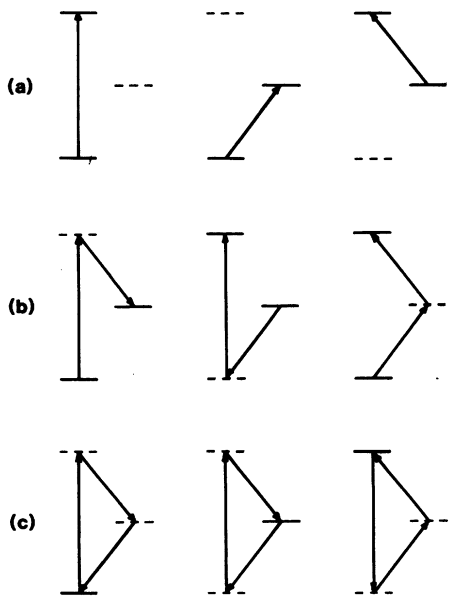

FIG. 2. Interactions involving (a) one, (b) two, and (c) three waves. Not shown are virtual transitions involving ordered pairs of these.

Of interest here is subsequent transitions between the upper and lower triplet manifolds, parametric transitions involving the triplets, and multiplet effects associated with a strong parametric field. These conditions and effects imply that all processes shown in Fig. 2 are important necessitating a nonperturbative analysis. Such an analysis can be made tractable with the use of a semiclassical approach in conjunction with selected approximations, most notably the rotating wave approximation.

The density matrix ρ can be resolved into two distinct, but not unrelated, elements, diagonal elements ρ_{ii}, which are fractional populations, and off-diagonal elements, ρ_{ij}, which control observables. Separate equations of motion for these follow from $\dot{\rho}=[H,\rho]/i\hbar$ and are

$$\dot{\rho}_{ii}=-\frac{\rho_{ii}-\rho_{ii}^{e}}{\tau_{ii}}+\sum_{k}\frac{\rho_{ik}\vec{\mu}_{ki}\cdot\vec{E}-\vec{\mu}_{ik}\cdot\vec{E}\rho_{ki}}{i\hbar}, \quad (1)$$

$$\dot{\rho}_{ij}=-\left(i\Omega_{ij}+\frac{1}{\tau_{ij}}\right)\rho_{ij}+\sum_{k}\frac{\rho_{ik}\vec{\mu}_{kj}\cdot\vec{E}-\vec{\mu}_{ik}\cdot\vec{E}\rho_{kj}}{i\hbar}, \quad (2)$$

where τ_{ii} and τ_{ij} are phenomenological T_1 and T_2 parameters, ρ_{ii}^{e} are equilibrium diagonal elements, $\Omega_{ij}=(E_i-E_j)/\hbar$, and electric dipole interactions are assumed.[31]

We assume that the system under consideration has mixed parity so that matrix elements exist between all states but that matrix elements of the form $\vec{\mu}_{ii}$ can be ignored since these do not cause transitions. With these and the linkage diagram of Fig. 1, Eq. (2) can be evaluated for the three off-diagonal elements ρ_{12}, ρ_{23}, and ρ_{13} yielding the equations of motion

$$\dot{\rho}_{12}=-(i\Omega_{12}+1/\tau_{12})\rho_{12}+[(\rho_{11}-\rho_{22})\vec{\mu}_{12}\cdot\vec{E}+\rho_{13}\vec{\mu}_{32}\cdot\vec{E}-\rho_{32}\vec{\mu}_{13}\cdot\vec{E}]/i\hbar, \quad (3)$$

$$\dot{\rho}_{23}=-(i\Omega_{23}+1/\tau_{23})\rho_{23}+[(\rho_{22}-\rho_{33})\vec{\mu}_{23}\cdot\vec{E}+\rho_{21}\vec{\mu}_{13}\cdot\vec{E}-\rho_{13}\vec{\mu}_{21}\cdot\vec{E}]/i\hbar, \quad (4)$$

$$\dot{\rho}_{13}=-(i\Omega_{13}+1/\tau_{13})\rho_{13}+[(\rho_{11}-\rho_{33})\vec{\mu}_{13}\cdot\vec{E}+\rho_{12}\vec{\mu}_{23}\cdot\vec{E}-\rho_{23}\vec{\mu}_{12}\cdot\vec{E}]/i\hbar, \quad (5)$$

and where $\rho_{ji}=\rho_{ij}^{*}$ follows from the Hermiticity of ρ.

Next, we assume an optical-like interaction involving copropagating traveling waves by setting

$$\vec{E}=\sum_{i=1}^{3}\vec{\mathcal{E}}_i\cos(\omega_i t-k_i z+\theta_i),$$

where θ_i are arbitrary phase factors and $\vec{\mathcal{E}}_i$ are time-independent amplitudes with implicit space dependence and polarization $\hat{\epsilon}_i$. Consistent with the near resonant nature of the interaction, we assume that, for example, ω_1 is sufficiently close to Ω_{21} so that the dominant Fourier coefficients of ρ_{12} are at ω_1 and $\omega_3-\omega_2$. Using this observation and the rotating-wave approximation, the dominant Fourier contribution to ρ_{ij} can be identified as

$$\rho_{12}=\tilde{\rho}_{12}^{a}e^{i(\omega_1 t-k_1 z)}+\tilde{\rho}_{12}^{b}e^{i[(\omega_3-\omega_2)t-(k_3-k_2)z]}, \quad (6)$$

$$\rho_{23}=\tilde{\rho}_{23}^{a}e^{i(\omega_2 t-k_2 z)}+\tilde{\rho}_{23}^{b}e^{i[(\omega_3-\omega_1)t-(k_3-k_1)z]}, \quad (7)$$

$$\rho_{13}=\tilde{\rho}_{13}^{a}e^{i[(\omega_1+\omega_2)t-(k_1+k_2)z]}+\tilde{\rho}_{13}^{b}e^{i(\omega_3 t-k_3 z)}, \quad (8)$$

where $\tilde{\rho}_{ij}^{l}$ are constants to be determined.[32] With these, the most general reductions of Eqs. (3)–(5) occurs when $\omega_3\neq\omega_1+\omega_2$.

Equations (3)–(5) are subsequently reduced to a set of algebraic equations by substituting in Eqs. (6)–(8), multiplying by the appropriate conjugate phase factors and using a short time average to eliminate rapidly oscillating terms. The resulting algebraic equations, twelve in number, are expressed in terms of complex Rabi frequencies $\Lambda_{12}=\vec{\mu}_{12}\cdot\vec{\mathcal{E}}_1 e^{i\theta_1}/2\hbar$, $\Lambda_{23}=\vec{\mu}_{23}\cdot\vec{\mathcal{E}}_2 e^{i\theta_2}/2\hbar$, $\Lambda_{13}=\vec{\mu}_{13}\vec{\mathcal{E}}_3 e^{i\theta_3}/2\hbar$ and complex detunings defined as

$$L_{12}^{a}=\Omega_{12}+\omega_1-i/\tau_{12},\quad L_{12}^{b}=\Omega_{12}+\omega_3-\omega_2-i/\tau_{12},$$
$$L_{23}^{a}=\Omega_{23}+\omega_2-i/\tau_{23},\quad L_{23}^{b}=\Omega_{23}+\omega_3-\omega_1-i/\tau_{23},$$
$$L_{13}^{b}=\Omega_{13}+\omega_3-i/\tau_{13},\quad L_{13}^{a}=\Omega_{13}+\omega_1+\omega_2-i/\tau_{13},$$

and are

$$L_{12}^{a}\tilde{\rho}_{12}^{a}=\tilde{\rho}_{32}^{b}\Lambda_{13}-\tilde{\rho}_{13}^{a}\Lambda_{23}^{*}-(\rho_{11}-\rho_{22})\Lambda_{12}, \quad (9)$$

$$L_{12}^{b}\tilde{\rho}_{12}^{b}=\tilde{\rho}_{32}^{a}\Lambda_{13}-\tilde{\rho}_{13}^{b}\Lambda_{23}^{*}, \quad (10)$$

$$L_{23}^{a}\tilde{\rho}_{23}^{a}=\tilde{\rho}_{13}^{a}\Lambda_{12}^{*}-\tilde{\rho}_{21}^{b}\Lambda_{13}-(\rho_{22}-\rho_{33})\Lambda_{23}, \quad (11)$$

$$L_{23}^{b}\tilde{\rho}_{23}^{b}=\tilde{\rho}_{13}^{b}\Lambda_{12}^{*}-\tilde{\rho}_{21}^{a}\Lambda_{13}, \quad (12)$$

$$L_{13}^{a}\tilde{\rho}_{13}^{a}=\tilde{\rho}_{23}^{a}\Lambda_{12}-\tilde{\rho}_{12}^{a}\Lambda_{23}, \quad (13)$$

$$L_{13}^{b}\tilde{\rho}_{13}^{b}=\tilde{\rho}_{23}^{b}\Lambda_{12}-\tilde{\rho}_{12}^{b}\Lambda_{23}-(\rho_{11}-\rho_{33})\Lambda_{13}. \quad (14)$$

The remaining six equations are the complex conjugate terms. For these, the complex detuning is defined as the negative of the conjugate detuning, for example, $L_{21}^{a}=-L_{12}^{a*}$, so that

$$L_{21}^{a}\tilde{\rho}_{21}^{a}=(\rho_{11}-\rho_{22})\Lambda_{12}^{*}-\tilde{\rho}_{23}^{b}\Lambda_{13}^{*}+\tilde{\rho}_{31}^{a}\Lambda_{23}.$$

The solution to this set of equations in which population differences appear as independent variables is listed in Appendix A.

The next step in the calculation involves the determination of the populations under the influence of the fields. For the linkage diagram in Fig. 1,

the population equations, Eq. (1), become

$$\dot{\rho}_{11}=-(\rho_{11}-\rho_{11}^{e})/\tau_{11} + 2\,\mathrm{Im}(\rho_{12}\vec{\mu}_{21}\cdot\vec{E}+\rho_{13}\vec{\mu}_{31}\cdot\vec{E})/\hbar=0, \quad (15)$$

$$\dot{\rho}_{22}=-(\rho_{22}-\rho_{22}^{e})/\tau_{22} + 2\,\mathrm{Im}(\rho_{23}\vec{\mu}_{32}\cdot\vec{E}-\rho_{12}\vec{\mu}_{21}\cdot\vec{E})/\hbar=0, \quad (16)$$

$$\dot{\rho}_{33}=-(\rho_{33}-\rho_{33}^{e})/\tau_{33} - 2\,\mathrm{Im}(\rho_{13}\vec{\mu}_{31}\cdot\vec{E}+\rho_{23}\vec{\mu}_{32}\cdot\vec{E})/\hbar=0. \quad (17)$$

Using Eqs. (6)–(8) and a short time average, the three driving terms in these equations become

$$\rho_{12}\vec{\mu}_{21}\cdot\vec{E}/\hbar\rightarrow\tilde{\rho}_{12}^{a}\Lambda_{12}^{*}+\tilde{\rho}_{12}^{b}\Lambda_{12}^{*}F, \quad (18)$$

$$\rho_{23}\vec{\mu}_{32}\cdot\vec{E}/\hbar\rightarrow\tilde{\rho}_{23}^{a}\Lambda_{23}^{*}+\tilde{\rho}_{23}^{b}\Lambda_{23}^{*}F, \quad (19)$$

$$\rho_{13}\vec{\mu}_{31}\cdot\vec{E}/\hbar\rightarrow\tilde{\rho}_{13}^{a}\Lambda_{13}^{*}F^{*}+\tilde{\rho}_{13}^{b}\Lambda_{13}^{*}, \quad (20)$$

where a phase factor F has been defined as

$$F=\exp\{i[(\omega_3-\omega_1-\omega_2)t-(k_3-k_1-k_2)z]\}. \quad (21)$$

The factor F clearly labels the parametric terms in Eqs. (18)–(20) and simply expresses the familiar degradation of the interaction if conservation of energy and momentum are both not satisfied between the interacting waves.

The solutions to Eqs. (15)–(17), which are performed numerically, are then used to determine the specific value of the off-diagonal elements under the influence of the three fields at some space point. Given these, the macroscopic polarization which drives the waves is found, as an observable, from $\vec{P}=N\,\mathrm{Tr}(\rho\vec{\mu})$ where N is the number density of three-level systems. Since $\vec{P}$ is real, the relevant complex polarizations are $\vec{P}_1=N\vec{\mu}_{21}\rho_{12}$, $\vec{P}_2=N\vec{\mu}_{32}\rho_{23}$, and $\vec{P}_3=N\vec{\mu}_{31}\rho_{13}$ where ρ_{ij} are given in Eqs. (6)–(8). Each polarization is thus seen to be comprised of parametric and nonparametric contributions. Before discussing the coupling of these polarizations to the waves, the multiphoton nature of the interaction in terms of saturation and level splittings will be illustrated.

III. LOCAL SOLUTIONS

Some insight into the relevant dynamics of the interactions can be gained by considering spatially localized solutions evaluated at $z=0$. For the case of a growth of $\vec{\mathcal{E}}_3$, what is desired is $\vec{P}_3=N\vec{\mu}_{31}\rho_{13}$ where ρ_{13} is given in Eq. (8). The various contributions to ρ_{13} implied by Eqs. (9)–(14) can be appreciated by representing these equations and the conjugate equations in the form of a signal flow graph introduced earlier for this application.[33,34]

The signal flow graph appropriate to these equations is shown in Fig. 3. The nodes represent the dependent variables (off-diagonal elements) and independent variables (diagonal elements). The nodes are connected by branches, each of which has a branch weight equal to a Rabi frequency. Each dependent variable node has an associated node weight equal to the complex detuning bearing the node label. Thus, the signal flow graph is a representation of the system of equations, Eqs. (9)–(14), of the form

(node weight)×(off-diagonal element)

$$=\sum(\text{branch weight})\times(\text{density-matrix element}),$$

where the arrow on the branch points from the nodes on the right-hand side of this equation to that on the left.

Aside from the ability to visualize a system of equations, one virtue of the signal flow graph is that a solution may be obtained directly from the graph using a set of simple rules and algorithms.[33] In our sense, a solution means expressing some off-diagonal element in terms of relevant diagonal

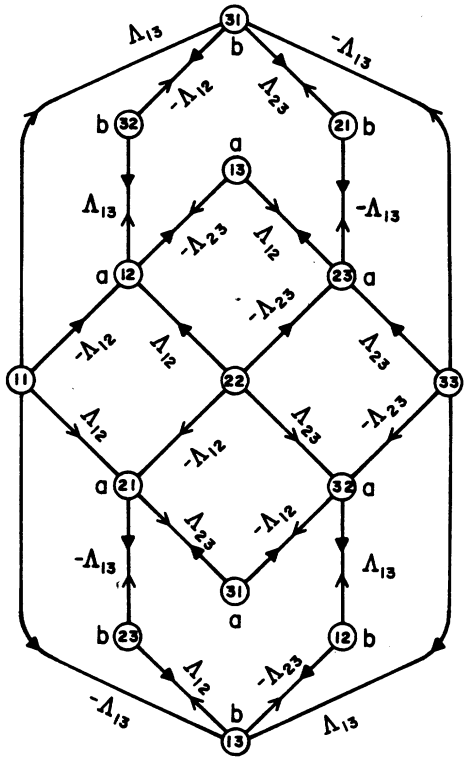

FIG. 3. Signal flow graph representation of Eqs. (9)–(14). The nodes are labeled according to the density-matrix elements and have an implied node weight equal to the complex detuning associated with the off-diagonal element. The Rabi frequencies are branch weights referring to the solid arrow. The open arrows refer to a branch weight equal to the conjugate of the indicated branch weights.

elements and some algebraic function entailing the Rabi frequencies and detunings. The solutions listed in Appendix A were in fact obtained from this graph using the rules listed elsewhere.[33] For our purpose here, we only consider the local solutions appropriate to a weak harmonic for both strong and weak pumping fields with the general case listed in Appendix A.

Associated with each branch is a "gain" or branch gain defined as the ratio of the branch weight to the terminal node weight. For example, in the lower part of the graph, the branch gain for the path $13^b \rightarrow 12^b$ is $-\Lambda_{23}^*/L_{12}^b$ while the reverse branch gain for the path $12^b \rightarrow 13^b$ is $-\Lambda_{23}/L_{13}^b$. A general path is comprised of a sequence of connected branches which may or may not be closed. A path gain is simply the product of branch gains. A solution is ultimately constructed by summing over all paths which connect a diagonal node to the off-diagonal node under consideration. Since closed paths may be traversed an infinite number of times, the solution expressed in closed form is equivalent to infinite order perturbation theory which necessarily includes strong-field level shifts and splittings.

A. Perturbation limit

The full perturbation limit can be achieved by considering only the contributions to the off-diagonal nodes associated with the shortest paths. Although the formalism presented so far is applicable to harmonic generation, sum and difference frequency generation, and parametric oscillators, we specialize at this point to the specific case of second-harmonic generation by setting $\omega_1=\omega_2$, $\vec{\mathcal{E}}_1=\vec{\mathcal{E}}_2$, $k_1=k_2$, and $\theta_1=\theta_2=0$. What is thus desired is

$$\vec{P}_3=N\vec{\mu}_{31}(\tilde{\rho}_{13}^a e^{i2\omega_1 t}+\tilde{\rho}_{13}^b e^{i\omega_3 t}). \tag{22}$$

From Fig. 3, $\tilde{\rho}_{13}^b$ is seen to be connected to the diagonal nodes via one- and three-branch paths. The former represents the one-photon transition $|1\rangle \rightarrow |3\rangle$ while the latter represents two-photon or Raman transitions for example $|1\rangle \rightarrow |2\rangle$. The perturbation limit for these is simply

$$\tilde{\rho}_{13}^b=\frac{\Lambda_{13}(\rho_{33}-\rho_{11})}{L_{13}^b}-\frac{\Lambda_{13}\Lambda_{12}^2(\rho_{11}-\rho_{22})}{L_{13}^b L_{23}^b L_{21}^a}$$

$$-\frac{\Lambda_{13}\Lambda_{23}^2(\rho_{22}-\rho_{33})}{L_{13}^b L_{12}^b L_{32}^a}, \tag{23}$$

in which the first term is the one-photon term.[35] For the parametric term, $\tilde{\rho}_{13}^a$, the shortest path is comprised of two branches yielding

$$\tilde{\rho}_{13}^a=\frac{\Lambda_{12}\Lambda_{23}}{L_{13}^a}\left(\frac{(\rho_{11}-\rho_{22})}{L_{12}^a}-\frac{(\rho_{22}-\rho_{33})}{L_{23}^a}\right). \tag{24}$$

These paths touch nodes 12^a, 13^a, and 23^a which are also common to the two-photon transition $|1\rangle \rightarrow |3\rangle$ so Eq. (24) is seen to be comprised of two-photon-like parts. The result in Eq. (24), which was previously derived by Andresen *et al.*[7,16] and by Voskanyan *et al.*,[9] is one of twelve possible contributions to the overall nonlinear susceptibility derived earlier by a diagrammatic perturbation technique.[3] However, because of the near resonant nature of the interaction, the result shown in this equation is the dominant term. The presence of the complex detunings shows that one resonant enhancement occurs when the pump is at least on two-photon resonance, $\Omega_{31}=2\omega_1$. If $\rho_{11}=\rho_{11}^e=1$, a second resonant enhancement condition occurs when the pump is also on one-photon resonance, $\Omega_{21}=\omega_1$. If $\rho_{11}=\rho_{11}^e\neq 1$, then the two terms in the bracket may interfere causing a local minimum in the nonlinear susceptibility with pump detuning. This interference effect has been predicted and discussed earlier and also observed experimentally.[7,8,9,16]

If $\rho_{11}=\rho_{11}^e=1$, $\tilde{\rho}_{13}^a$ approaches a maximum value of

$$\tilde{\rho}_{13}^a|_{\max} \rightarrow -\tau_{13}\tau_{12}\Lambda_{12}\Lambda_{23} \sim |\vec{\mathcal{E}}_1|^2,$$

which shows that the nonlinear polarization may be increased by increasing the pump field. This increase will eventually saturate due to two reasons; population saturation and strong-field level splittings to be discussed next.

B. Strong-pump limit

The strong-pump limit is obtained by adding to the previous solutions, contributions from higher-order (longer) paths with branch weights equal to Λ_{12} or Λ_{23}. This involves only closed paths of the form $13^a \rightarrow 23^a \rightarrow 13^a$ which are equivalent to virtual transitions.[33,34] The summation converges to a continued fraction form and can be solved for directly using the graph algebra or deduced from the general solution in Appendix A in the limit $\Lambda_{13} \rightarrow 0$.

If the pump is strong and near resonance, states $|1\rangle$, $|2\rangle$, and $|3\rangle$ are tightly coupled and each splits into a triplet.[23,24,30] Transitions associated with ω_3 will then be between the upper and lower triplet manifolds. An important feature of the solutions is the inclusion of the location and strength of the transition between these dressed states as will now be shown.

We find it convenient to decompose $\tilde{\rho}_{13}^b$ into one-photon $\tilde{\rho}_{13}^b|_1$ and two-photon-like $\tilde{\rho}_{13}^b|_2$ contributions.[35] In the limit $\Lambda_{13} \rightarrow 0$, terms lowest order in Λ_{13} are retained so that the one-photon result becomes

$$\tilde{\rho}^{b}_{13}|_1=\frac{\Lambda_{13}(\rho_{33}-\rho_{11})}{L^{b}_{13}\left(1-\frac{\Lambda^2_{12}}{L^{b}_{13}L^{b}_{23}}-\frac{\Lambda^2_{23}}{L^{b}_{13}L^{b}_{12}}\right)}\,, \tag{25}$$

which is modified slightly from the equivalent term in Eq. (23). The implication of this result can be seen by treating $\vec{\mathcal{E}}_3$ as a tunable probe wave by setting as a variable $Z=\Omega_{31}-\omega_3$ [see Fig. 1(b) for the field and detuning notation]. Resonances sensed by $\vec{\mathcal{E}}_3$ then occur at detunings, Z, for which the denominator in Eq. (25) becomes purely complex, or the real part becomes zero.[36] To deduce the location of these resonances, set $X=\Omega_{21}-\omega_1$ and $Y=\Omega_{32}-\omega_1$ and recast the denominator of Eq. (25) into an algebraic equation by setting the i/T_2 terms to zero; the so-called sharp-line limit. With these, resonances are the roots of

$$Z(Z-X)(Z-Y)-\Lambda^2_{12}(Z-Y)-\Lambda^2_{23}(Z-X)=0\,, \tag{26}$$

which is clearly cubic implying at most three resonances. If the pump is on two-photon and one-photon resonance ($X=Y=0$), the roots are simple to obtain and are

$$Z=\Omega_{31}-\omega_3=\pm\,(\Lambda^2_{12}+\Lambda^2_{23})^{1/2}, \tag{27}$$

which is the two-photon analog of Autler-Townes splitting.[27] This result is very significant because it shows that at full resonance, the $|1\rangle\rightarrow|3\rangle$ transition is split into a doublet, thus minimizing absorption of the growing harmonic which satisfied the parametric resonance condition on line center, $Z=0$.[37] This conclusion is independent of the values of ρ_{ii} in Eq. (25).

Similarly, the two-photon contributions can be obtained as

$$\begin{aligned}\tilde{\rho}^{b}_{13}|_2=&-(\rho_{11}-\rho_{22})\frac{\Lambda_{13}}{L^{a}_{21}}\left[\frac{\Lambda^2_{12}}{L^{b}_{23}L^{b}_{13}}\left(1-\frac{\Lambda^2_{12}}{L^{a}_{31}L^{a}_{32}}\right)-\frac{\Lambda^2_{12}\Lambda^2_{23}}{L^{a}_{31}L^{a}_{32}L^{b}_{12}L^{b}_{13}}\right]\frac{1}{\Delta}\\&-(\rho_{22}-\rho_{33})\frac{\Lambda_{13}}{L^{a}_{32}}\left[\frac{\Lambda^2_{23}}{L^{b}_{12}L^{b}_{13}}\left(1-\frac{\Lambda^2_{23}}{L^{a}_{21}L^{a}_{31}}\right)-\frac{\Lambda^2_{12}\Lambda^2_{23}}{L^{a}_{31}L^{a}_{21}L^{b}_{23}L^{b}_{13}}\right]\frac{1}{\Delta}\,,\end{aligned} \tag{28}$$

where

$$\begin{aligned}\Delta=&(1-\Lambda^2_{23}/L^{a}_{21}L^{a}_{31}-\Lambda^2_{12}/L^{a}_{31}L^{a}_{32})\\&\times(1-\Lambda^2_{12}/L^{b}_{23}L^{b}_{13}-\Lambda^2_{23}/L^{b}_{13}L^{b}_{12})\,.\end{aligned}$$

These again are modifications of the form shown in Eq. (23) and have resonances which are similar to those just discussed.

Finally, the parametric term can be reduced to

$$\begin{aligned}\tilde{\rho}^{a}_{13}=&\frac{\Lambda_{12}\Lambda_{23}}{L^{a}_{13}}\left(\frac{(\rho_{11}-\rho_{22})}{L^{a}_{12}}-\frac{(\rho_{22}-\rho_{33})}{L^{a}_{23}}\right)\\&\times\frac{1}{\left(1-\frac{\Lambda^2_{23}}{L^{a}_{12}L^{a}_{13}}-\frac{\Lambda^2_{12}}{L^{a}_{13}L^{a}_{23}}\right)}\,.\end{aligned} \tag{29}$$

This equation was also derived by Voskanyan *et al.*,[9] but evaluated by them in the perturbation limit by setting $\Lambda^2_{ij}\rightarrow 0$. Since the detunings in this equation are independent of Z, this function has an implied parametric resonance when $\omega_3=2\omega_1$ or $Z=X+Y$. Both numerator and denominator are proportional to $\mathcal{E}^2_1$ so that in the strong field limit $\tilde{\rho}^{a}_{13}$ must saturate. This can be seen for the case of full resonance for which

$$\begin{aligned}\tilde{\rho}^{a}_{13}=&-\frac{\Lambda_{12}\Lambda_{23}\tau_{13}\tau_{12}}{1+\Lambda^2_{23}\tau_{12}\tau_{13}+\Lambda^2_{12}\tau_{13}\tau_{23}}\\&\times\left((\rho_{11}-\rho_{22})-\frac{\tau_{23}}{\tau_{12}}(\rho_{22}-\rho_{33})\right).\end{aligned} \tag{30}$$

For roughly equal matrix elements and T_2 values, the multiplier to this equation saturates at one-half. Therefore the saturated value of $\tilde{\rho}^{a}_{13}$ will be controlled predominantly by the saturated values of the populations. The population term may, depending on conditions, saturate at a positive or negative value or even be zero. As a simple example, if all matrix elements T_2 and T_1 values are equal, the parametric term can be evaluated from Eqs. (B1) and (B2) and shown to saturate to

$$\tilde{\rho}^{a}_{13}=-\tfrac{1}{8}\left[(\rho^{e}_{11}-\rho^{e}_{22})-(\rho^{e}_{22}-\rho^{e}_{33})\right], \tag{31}$$

and indicates that even under fully saturated conditions, the parametric contribution does not necessarily disappear and that temperature reduces the magnitude of the coefficient.

C. Variable scans

The relevant dynamics implied by the multiphoton nature of the interaction, including saturation, can be further illustrated with graphs of the off-diagonal elements. For these we simply take all T_1 and T_2 values equal and specify all frequencies and detunings in units of T_2. Of interest are the absorption, dispersion, and parametric contributions under various pumping field conditions, but for a weak harmonic. For the nonparametric term, $\tilde{\rho}^{b}_{13}$, from Eq. (20) it can be seen that the absolute phase of $\vec{E}_3$ does not enter since $\tilde{\rho}^{b}_{13}\sim\Lambda_{13}$. Hence, normalized absorption and dispersion functions are defined as the imaginary and real parts of $\tilde{\rho}^{b}_{13}/\Lambda_{13}$

with extrema of ±1 and ±0.5, respectively. For the parametric term, we replace F at $z=0$ by a Lorentzian

$$F=e^{i(\omega_3-\omega_1-\omega_2)t} = e^{i(\omega_3-2\omega_1)t} \rightarrow \frac{\delta^2}{(\omega_3-2\omega_1)^2+\delta^2}=g_R, \tag{32}$$

where δ is chosen to be one-tenth the width of one transition. Further, as will be seen in the next section, the phase θ_3 adjusts itself so that the absolute magnitude of $\tilde{\rho}^q_{13}$ determines the initial parametric field growth. This leads us to consider a parametric function $|\tilde{\rho}^q_{13}g_R|$ in the limit as $\Lambda_{13}\rightarrow 0$. The norm on this function is one-half. The three functions are readily evaluated from Eqs. (25), (28), and (29) using the diagonal elements determined from the numerical solution of Eqs. (15)–(17) outlined in Appendix B.

In Fig. 4 are shown graphs of these functions for various pump detunings versus the ω_3 detuning. The arrows on the lower part of the figure show the location of the resonances as determined from Eq. (26). Figure 4(a) shows the absorption doublet and a large parametric contribution on line center. The dispersion is also zero on exact parametric resonance as expected for a fully resonant situation. Figure 4(b) shows the splitting of the absorption doublet into a triplet when the pump is on two-photon resonance only. There is now a noticeable absorption and dispersion on parametric resonance. Figure 4(c) is the case when the pump is on one-photon resonance showing dispersion and absorption on parametric resonance. Figure 4(d) is for no pump resonances and shows a reduction in the magnitude of the parametric term as expected from the considerations in the last section.

The saturation behavior is illustrated in Fig. 5 for the case of full resonance. Also shown are the values of the diagonal elements. It is evident that relatively low fields are required to saturate the system and that because of saturation, the medium is transparent to the harmonic and, most importantly, the parametric term saturates to a nonzero value. For reference purposes, $4(\Lambda_{ij}T_2)^2 = I/I_{\text{sat }ij}$, where I and $I_{\text{sat }ij}$ are the field intensity and saturation intensity for the $|i\rangle\rightarrow|j\rangle$ transi-

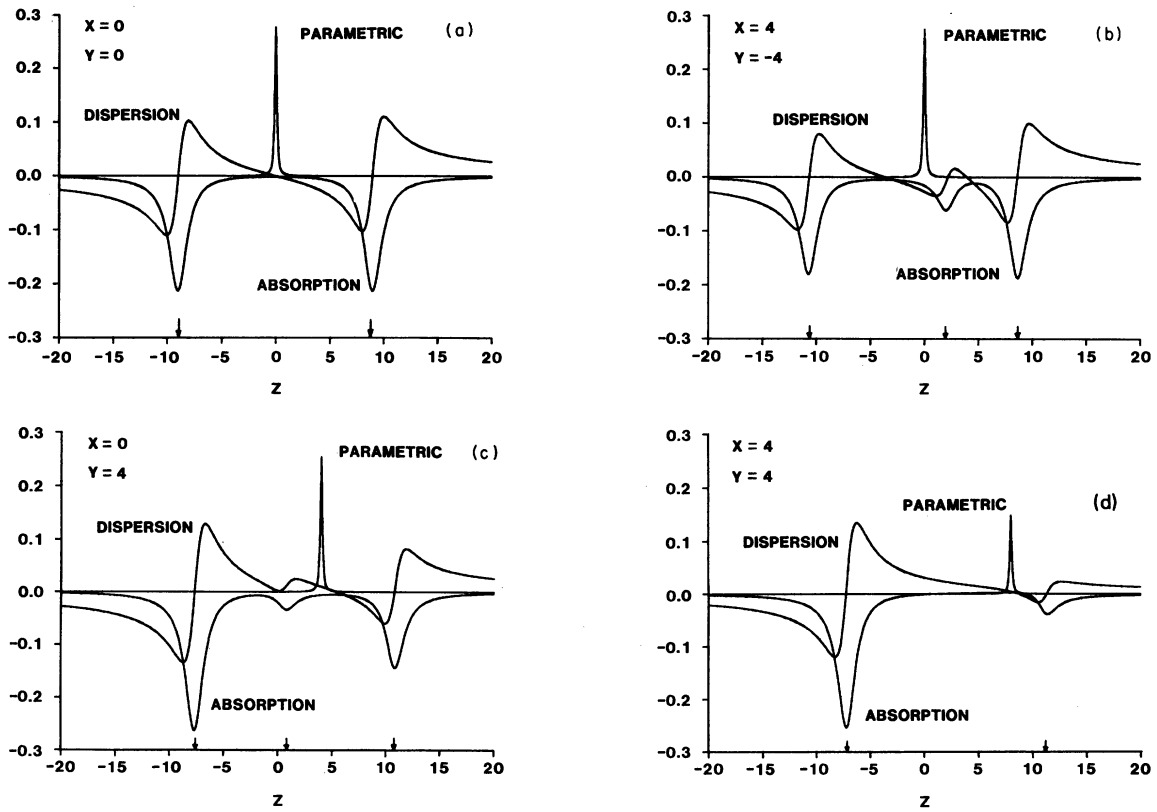

FIG. 4. Numerical solutions showing the dispersion, absorption, and parametric gain versus detuning $Z=(\Omega_{31}-\omega_3)T_2$. In all cases, $\rho^e_{11}=1$, $T_1=T_2$, $\Lambda_{12}T_2=4$, $\Lambda_{23}T_2=8$. (a) $X=Y=0$, (b) $X=-Y=4$, (c) $X=0$, $Y=4$, and (d) $X=Y=4$. Arrows show the location of the resonances from Eq. (26).

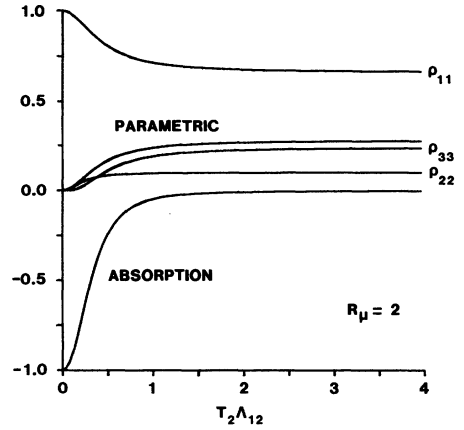

FIG. 5. Saturation behavior of the absorption and parametric gain for $X=Y=Z=0$, $\rho_{11}^e=1$, $T_1=T_2$, and $R_\mu=2$ versus $\Lambda_{12}T_2$. Also shown are the saturated diagonal elements.

tion, respectively.

As indicated in the last section, the parametric contribution associated with $|2\rangle$ enters in with a sign opposite to the contributions from $|1\rangle$ and $|3\rangle$ as can be seen in Eq. (29). This causes an interference effect which can destroy the parametric term under certain conditions. This interference effect is illustrated in Fig. 6 which contains graphs of the parametric and nonparametric terms versus the intermediate detuning (X or Y) for parametric ($Z=X+Y$) and two-photon resonance ($X+Y=0$). The graphs correspond to a ratio $R_\mu=\Lambda_{23}/\Lambda_{12}=\hat{\epsilon}_1\cdot\vec{\mu}_{23}/\hat{\epsilon}_1\cdot\vec{\mu}_{12}$, varying from 0 to 2. What is indirectly being varied in these graphs is the saturated value of the elements ρ_{22} and ρ_{33}. The existence of the dip, previously predicted in the perturbation limit [Eq. (24)] and observed,[7,8,9,16] is seen to be dependent on the matrix element ratio. The worst possible case occurs when $R_\mu\cong 1/\sqrt{2}$ for which $|\tilde{\rho}_{13}^a g_R|=0$.

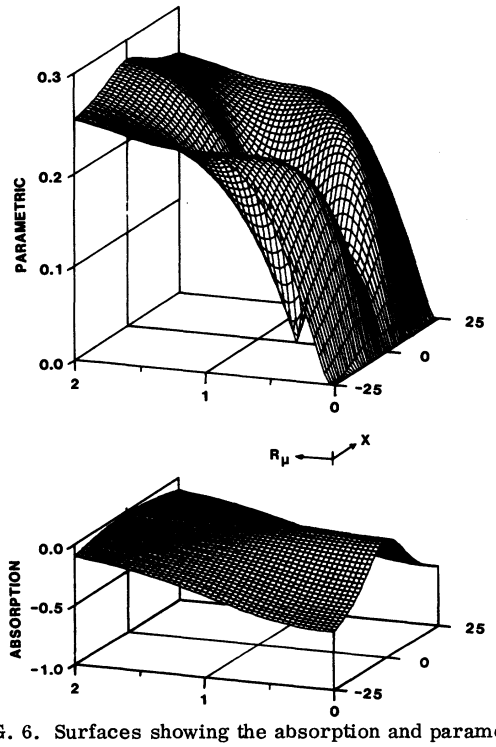

FIG. 6. Surfaces showing the absorption and parametric gain versus intermediate detuning X and R_μ. For these $\rho_{11}^e=1$, $X+Y=Z=0$, and $\Lambda_{12}T_2=4$. From these, the parametric gain has local maxima at $X=0$, $R_\mu=0.35$ and 2, and $X=\pm 25$, $R_\mu\cong 1/\sqrt{2}$.

The absorption, determined predominantly by $\rho_{11}-\rho_{33}$, exhibits severe power broadening because the pump is strong and on two-photon resonance. From this figure, if $R_\mu\leq\sqrt{2}$, a maximum parametric gain exists for X detunings where there is a strong harmonic absorption. In the opposite case for $R_\mu>\sqrt{2}$, the maximum parametric gain occurs on full resonance wherein the absorption is small.

The matrix element dependence of the parametric gain is further illustrated in Fig. 7. For this figure, full resonance is assumed and the matrix element ratio R_μ is again varied. Also shown in this figure is the multiplier to the population difference term in Eq. (30) which determines the maximum value of the parametric off-diagonal element. The asymptotic approach of $|\tilde{\rho}_{13}^a g_R|$ to the value of the multiplier is indicative of a *reduction* in saturation. This can be understood as follows. If $\Lambda_{23}\gg\Lambda_{12}$, the ac Stark splittings are determined mainly by Λ_{23}, in which case $|2\rangle$ and $|3\rangle$ are split into doublets. This also splits the $|1\rangle\rightarrow|3\rangle$ and $|1\rangle\rightarrow|2\rangle$ transitions into doublets making the media transparent to the harmonic *and* the pump. Hence under this idealized condition, there is no population saturation if $\rho_{11}^e=1$. If $\rho_{11}^e\neq 1$, then $\rho_{22}\rightarrow\rho_{33}\cong(\rho_{22}^e+\rho_{33}^e)/$

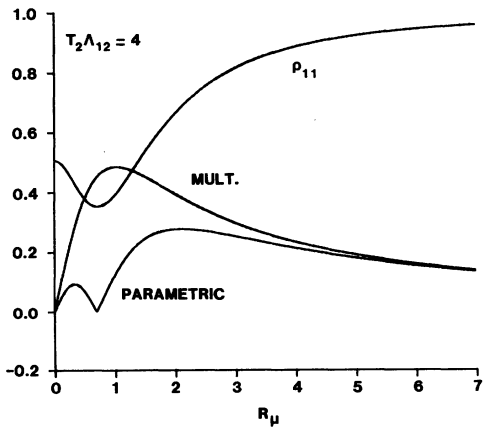

FIG. 7. Graph of the $X=0$ region of Fig. 6 versus R_μ. The multiplier (mult.) is $T_2^2\Lambda_{12}\Lambda_{23}/(1+T_2^2\Lambda_{12}^2+T_2^2\Lambda_{23}^2)$ as shown in Eq. (30).

2, so that $(\rho_{11}-\rho_{22})-(\rho_{22}-\rho_{33}) \rightarrow (3\rho_{11}^{e}-1)/2$ which is never zero for realistic temperatures.

Because of the saturated behavior of the parametric nonlinearity, it is not particularly fruitful to speak of a susceptibility in order to appreciate the magnitude of the effect. The magnitude can, instead, be compared with the magnitude of the one-photon absorption contained in $\tilde{\rho}_{13}^{b}$. This element will be large only in the absence of the pump and on line center. For arbitrary Λ_{13}, the element is easily shown to be $\tilde{\rho}_{13}^{b}=-i\Lambda_{13}\rho_{11}^{e}/(1+4\Lambda_{13}^{2})$, which has a norm of 0.25. Hence, in terms of a nonlinear polarization, the fully resonant case can have a second harmonic polarization as large as the largest one-photon polarization.

The finite value of $|\tilde{\rho}_{13}^{q}g_{R}|$ under saturated conditions is a consequence of the nonequal value of the saturated populations. The decay and dephasing elements, τ_{ii} and τ_{ij}, are also known to yield nonequal saturated populations when treated as variables.[23-26] Since the values of these parameters and the detailed form of the T_1 relaxation terms in Eqs. (15)–(17) tend to become system dependent, we continue to take $\tau_{ii}=\tau_{ij}=T_2$ and remark that the results to follow may vary from system to system for a fixed R_{μ} value.

The remaining terms in the ρ_{ij} elements in Appendix A containing higher powers of Λ_{13} must be responsible for level shifts and splittings caused by a strong harmonic.[38] Selected limits can be extracted from these equations, and will only be illustrated later for the case of parametric oscillation.

IV. EXTENDED SOLUTIONS

The results of the last section are very encouraging in the sense that even for the case of saturating fields on full resonance, harmonic absorption is weak and a nominal parametric gain exists. The next step is to consider the conversion dynamics under propagation conditions. Although most experiments have been performed in sample sizes dimensionally comparable to the pump wavelength and wherein dielectric feedback is present, we shall investigate an optical-like situation comprised of two copropagating traveling waves interacting in a dimensionally long sample with no host dispersion effects. This is clearly a gross approximation to the experiments to date, but it permits some insight to be gained into the relevant dynamics and the strength of the conversion.

A. Propagation paradigm

For the stated model situation, propagation effects are most easily treated using Maxwell's equations simplified by the slowly varying amplitude and phase approximations appropriate to optical interactions. With these, Maxwell's equations reduce to a single wave equation, for an assumed field $\vec{E}=\vec{\mathcal{E}}(z,t)e^{i(\omega t-kz)}$, given by

$$k\frac{\partial\vec{\mathcal{E}}}{\partial z}+\frac{k_{\infty}}{v_{p}}\frac{\partial\vec{\mathcal{E}}}{\partial t}+\frac{i}{2}(k_{\infty}^{2}-k^{2})\vec{\mathcal{E}}=\frac{i\mu_{0}}{2}\frac{\partial^{2}\vec{P}_{NL}}{\partial t^{2}}e^{-i(\omega t-kz)}, \tag{33}$$

where k_{∞} and v_p are the high-frequency wave vector and phase velocity and where $\vec{k}\cdot\vec{\mathcal{E}}=0$ has been assumed. For two waves, there are two such equations of the form of Eq. (33) which are coupled via the nonlinear polarization, $\vec{P}_{NL}$. For the case of the growth of the harmonic, $\vec{\mathcal{E}}=\vec{\mathcal{E}}_{3}e^{i\theta_3}/2$,

$$\vec{P}_{NL}=\vec{P}_{3}=N\vec{\mu}_{31}(\tilde{\rho}_{13}^{q}e^{i(2\omega_1 t-2k_1 z)}+\tilde{\rho}_{13}^{b}e^{i(\omega_3 t-k_3 z)}),$$

and the phase factor appearing on the right-hand side of Eq. (33) is $e^{-i(\omega_3 t-k_3 z)}$. Using these, the driving term for $\vec{\mathcal{E}}_3$ becomes

$$\frac{i\mu_{0}}{2}\frac{\partial^{2}\vec{P}_{NL}}{\partial t^{2}}e^{-i(\omega_3 t-k_3 z)}=-\frac{i\mu_{0}N\vec{\mu}_{31}}{2}(\omega_{3}^{2}\tilde{\rho}_{13}^{b}+4\omega_{1}^{2}\tilde{\rho}_{13}^{q}F^{*}), \tag{34}$$

where F is given by Eq. (21). In order to have an appreciable growth, F should be real, requiring a phase matched condition $k_3=2k_1$ and conservation of energy $\omega_3=2\omega_1$. In order to avoid complications of phase matching and index effects associated with the dispersion evident in Figs. 4(b)–4(d), in what follows we shall assume a perfect phase matched condition and that $k_i=k_{\infty}$. This clearly oversimplifies the situation, but yields information about the conversion under the "best of conditions." With this assumption, F and F^* are replaced by g_R in Eq. (32) to account for conservation of energy associated with the parametric interaction. Dotting Eq. (33) with $\vec{\mu}_{13}\cdot\hat{\epsilon}_{3}\hat{\epsilon}_{3}/\hbar$, the harmonic field growth is thus governed by

$$\frac{d}{dz}|\Lambda_{13}|=\frac{k_3|\vec{\mu}_{13}\cdot\hat{\epsilon}_{3}|^{2}N}{4\hbar\epsilon}\,\mathrm{Re}[-i(\tilde{\rho}_{13}^{b}+\tilde{\rho}_{13}^{q}g_{R})e^{-i\theta_3}]. \tag{35}$$

B. Phase paradigm

The phase θ_3 which was introduced as an independent parameter, has a well-defined value for parametric effects.[2] From the simple results for $\tilde{\rho}_{13}^{b}$ and $\tilde{\rho}_{13}^{q}$ in Eqs. (23) and (24), the choice of phase has no effect on the product $\tilde{\rho}_{13}^{b}e^{-i\theta_3}$ because $\tilde{\rho}_{13}^{b}\sim\Lambda_{13}\sim e^{i\theta_3}$. Hence θ_3 is chosen such that $-i\tilde{\rho}_{13}^{q}g_{R}e^{-i\theta_3}$ is purely real and positive. In the general case treated here, the parametric term $\tilde{\rho}_{13}^{q}$ is complex so that θ_3 has to be specified as an initial condition for each set of field values and

detunings. The general complex nature of the parametric nonlinearity was also pointed out by Inaba for the case of resonant difference frequency mixing.[11] The optimum phase can be specified as

$$\theta_3=\tan^{-1}\left(\frac{\mathrm{Im}(\tilde{\rho}^a_{13})}{\mathrm{Re}(\tilde{\rho}^a_{13})}\right)-\pi/2 \tag{36}$$

and has four special limits. If $\tilde{\rho}^a_{13}$ is purely real and positive (negative) $\theta_3=-\pi/2$ ($\pi/2$). If $\tilde{\rho}^a_{13}$ is purely imaginary and positive (negative), $\theta_3=0$ ($\pm\pi$). For the case of normal bulk harmonic generation, $\tilde{\rho}^a_{13}$ is positive and real while for the fully resonant case, $\tilde{\rho}^a_{13}$ is real but of either sign as seen in Eq. (24). Under optimum phase conditions, $\mathrm{Re}(-i\tilde{\rho}^a_{13}g_R e^{-i\theta_3})=|\tilde{\rho}^a_{13}g_R|$.

C. Propagation

We find it convenient to introduce a dimensionless space variable $\zeta=k_1N|\hat{\epsilon}_1\cdot\vec{\mu}_{12}|^2z/4\hbar\epsilon$ which has the significance that $\zeta T_2=\alpha_{12}z/2$ where α_{12} is the line center Beer's coefficient for the $|1\rangle\rightarrow|2\rangle$ transition. Thus, when the Rabi frequencies are expressed in units of T_2, ζ measures the distance in units of field Beer's coefficient. In terms of this variable, the coupled field equations become

$$\frac{d|\Lambda_{13}|}{d\zeta}=R_\alpha\,\mathrm{Re}[-i(\tilde{\rho}^b_{13}+\tilde{\rho}^a_{13}g_R)e^{-i\theta_3}]\,, \tag{37}$$

$$\frac{d\Lambda_{12}}{d\zeta}=\mathrm{Re}[-i(\tilde{\rho}^a_{12}+\tilde{\rho}^b_{12}g_R)-iR_\mu(\tilde{\rho}^a_{23}+\tilde{\rho}^b_{23}g_R)]\,, \tag{38}$$

where $R_\alpha=k_3|\hat{\epsilon}_3\cdot\vec{\mu}_{13}|^2/k_1|\hat{\epsilon}_1\cdot\vec{\mu}_{12}|^2$, $R_\mu=\hat{\epsilon}_1\cdot\vec{\mu}_{32}/\hat{\epsilon}_1\cdot\vec{\mu}_{12}$, and where θ_3 is fixed by the value at $\zeta=0$ determined from Eq. (36). If all matrix elements are equal and parallel, $R_\alpha=2$ and $R_\mu=1$. The graphs to follow will show normalized intensities defined as pump intensity I_p and harmonic intensity I_h:

$$I_p=\left(\frac{\Lambda_{12}(\zeta)}{\Lambda_{12}(0)}\right)^2=\frac{|\vec{\mathcal{E}}_1(\zeta)|^2}{|\vec{\mathcal{E}}_1(0)|^2}\,, \tag{39}$$

$$I_h=\left(\frac{|\Lambda_{13}(\zeta)|^2}{\Lambda_{12}(0)}\right)\frac{2}{R_\alpha}=\frac{|\vec{\mathcal{E}}_3(\zeta)|^2}{|\vec{\mathcal{E}}_1(0)|^2}\,, \tag{40}$$

where $2/R_\alpha$ in Eq. (40) scales $|\Lambda_{13}(\zeta)|^2$ into the same strength units as $\Lambda^2_{12}(0)$. With these, the intensities are normalized to unity. The propagation model is thus comprised of Eqs. (37) and (38), the phase paradigm in Eq. (36), and the full equations listed in Appendices A and B, all of which are integrated numerically.

Some insight into the conversion can be gained by considering special cases for which analytical solutions may be obtained. First, we recall the case of normal second-harmonic generation in transparent media under phase-matched conditions for which the growth is governed by

$$I_h=\tanh^2(a|\vec{\mathcal{E}}_1(0)|z)\,, \tag{41}$$

where a is some collection of constants.[2] If the argument is one, $I_h=0.58$ which occurs at $z=1/a|\vec{\mathcal{E}}_1(0)|$ and shows that an increase in initial pump intensity shortens the conversion distance. For large and small arguments, $I_h\rightarrow 1$ and $I_h\rightarrow a^2|\vec{\mathcal{E}}_1(0)|^2z^2$ and shows the full conversion capability of the process which has an initial parabolic growth. Next, consider fully resonant second-harmonic generation with $\rho^e_{11}=1$ and with very weak fields. In this limit the conversion is expected to be small so that the pump undergoes a simple exponential decay $\Lambda_{12}(\zeta)=\Lambda_{12}(0)\exp(-\zeta)$. Using the perturbation-limit results, Eqs. (23) and (24), for $\tilde{\rho}^a_{13}$ and $\tilde{\rho}^b_{13}$ in Eq. (37) yields

$$I_h=\frac{2}{R_\alpha}\left(\frac{R_\alpha R_\mu\Lambda_{12}(0)}{R_\alpha-2}(e^{-2\zeta_m}-e^{-R_\alpha\zeta_m})\right)^2\,, \tag{42}$$

for the maximum harmonic intensity which occurs at $\zeta_m=\ln(R_\alpha/2)/(R_\alpha-2)$. As a consequence of both pump and harmonic absorption, the conversion distance is limited to the smaller value of the reciprocal Beer's coefficient for the pump or the harmonic. For the special case of $R_\alpha=2$, $\zeta_m=1/2$, and $I_h=[R_\mu\Lambda_{12}(0)/e]^2$. In the very strong pump limit, the system is saturated so that $\tilde{\rho}^a_{13}\rightarrow$ constant and $\tilde{\rho}^b_{13}\sim 0$ because of Stark splitting. The pump will thus undergo an initial linear decay characteristic of a fully saturated, homogeneously broadened system. Since there is no absorption, the initial harmonic growth is found to be given by

$$I_h\cong\frac{2}{R_\alpha}\left(\frac{R_\alpha|\tilde{\rho}^a_{13}|\zeta}{\Lambda_{12}(0)}\right)^2\,, \tag{43}$$

indicating a parabolic growth. The harmonic will continue to grow ultimately to a point where pump depletion, saturation and harmonic field induced level shifts become important. For sufficiently long interaction distances, the pump will be fully depleted and the harmonic will decay in a linear fashion if it is saturating. All these features will be illustrated in the next two figures.

Some examples of the conversion of the pump into a second harmonic are shown in Fig. 8. Figure 8(a) illustrates a R_μ value far to the right of the peak in Fig. 7. In this case, Λ_{23} is so large that the $|1\rangle\rightarrow|2\rangle$ and $|1\rangle\rightarrow|3\rangle$ transitions are split out of resonance with the fields leaving most of the population in the ground state. In this case, the growth of the harmonic can be estimated directly from Eq. (43) by setting $|\tilde{\rho}^a_{13}|\simeq T_2^2\Lambda_{12}\Lambda_{23}/(1+T_2^2\Lambda_{12}^2+T_2^2\Lambda_{23}^2)\cong 0.16$ yielding $I_h\cong(0.16\zeta)^2$, which is plotted as dots in Fig. 8(a) and illustrates

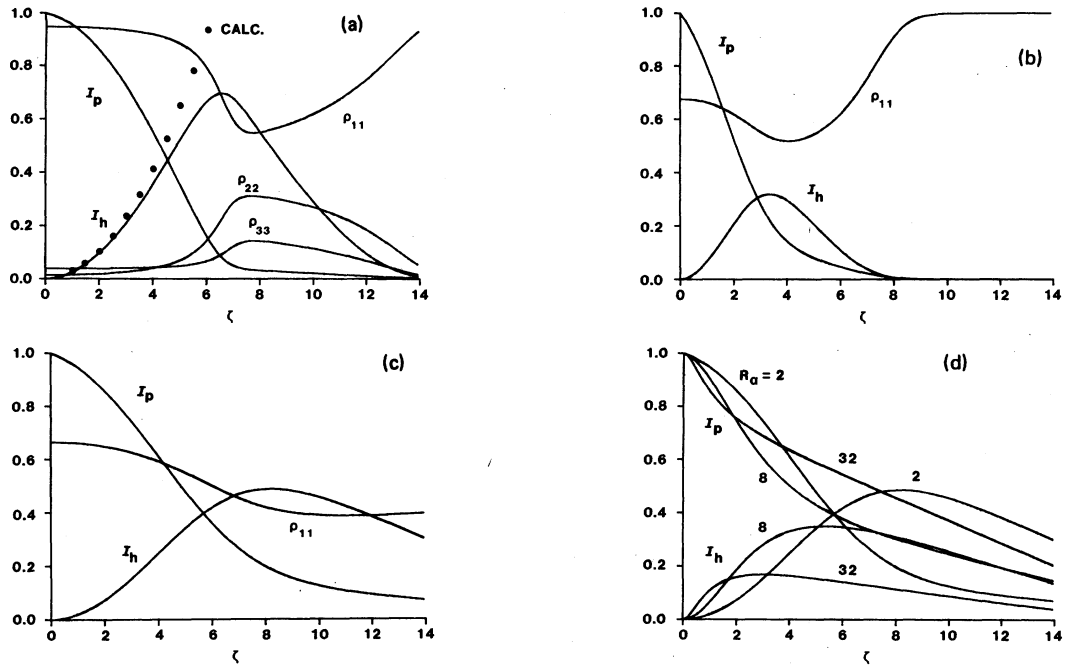

FIG. 8. Numerical solution of the coupled Maxwell equations for $\rho^0_{11}=1$, $X=Y=Z=0$. (a) $\Lambda_{12}T_2=2$, $R_\mu=6$ and calc. refers to the parabolic result in Eq. (43). (b) $\Lambda_{12}T_2=2$, $R_\mu=2$, (c) $\Lambda_{12}T_2=4$, $R_\mu=2$, (d) $\Lambda_{12}T_2=4$, $R_\mu=2$, and $R_\alpha=2,8,32$ corresponding to $\vec{\mu}_{13}\cdot\hat{\epsilon}_3/\vec{\mu}_{12}\cdot\hat{\epsilon}_1=1,2,4$.

the initial parabolic growth characteristic of a constant nonlinear polarization. As the pump and harmonic evolve, the nature of the interaction changes from harmonic growth to loss. For $\zeta>7$, the harmonic now drives the system via degenerate one-, two- and three-photon processes. The anomalously slow decay of the pump in this region is caused by this. The most interesting result is in the conversion efficiency which reaches 71% for this example.

Figures 8(b) and 8(c) illustrate the effect of an increasing pump field on the conversion. Since the initial pump field is saturating in both cases, the initial harmonic intensity ($|\vec{\mathcal{E}}_3|^2$) growth is the same. Consequently, for a larger pump, pump saturation can be maintained over a longer distance resulting in a larger harmonic intensity I_h. This behavior is evident in Fig. 8(b) and 8(c) and is just the opposite behavior observed in nonresonant second-harmonic generation implied in Eq. (41).

Figure 8(d) illustrates the effect of increasing $R_\alpha=k_3|\vec{\mu}_{13}\cdot\hat{\epsilon}_3|^2/k_1|\vec{\mu}_{12}\cdot\hat{\epsilon}_1|^2$ on the conversion. As implied by Eqs. (37) and (43) the harmonic growth scales as R_α so increasing this results in a faster growing harmonic which saturates at a smaller conversion efficiency. This is understandable in that for a large matrix element $\vec{\mu}_{13}\cdot\hat{\epsilon}_3$, less field is needed to cause saturation which results in a smaller conversion.

In Fig. 9 are shown graphs of I_h and the conversion distance ζ_m for various Λ_{12} and R_μ values. These results show that the highest conversion efficiency is achieved under conditions of strong saturation requiring increasingly longer interaction distances with increasing pumping intensity, both of which are understandable from the previous

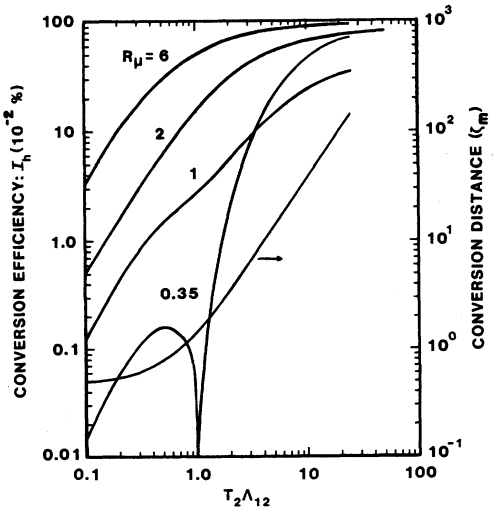

FIG. 9. Conversion efficiency and conversion distance ζ_m versus $\Lambda_{12}T_2$ for various R_μ. Only ζ_m values for $R_\mu=1$ are shown, the others being within a factor of 2 of these. For all cases $X=Y=Z=0$, $\rho^0_{11}=1$, and $R_\alpha=2$.

discussion. The remarkable result is in the very high conversion achieved for large R_μ implying that the resonant interaction can, in principle, be as efficient as in transparent media.

The curve for $R_\mu = 0.35$ is most unusual and is caused by a population interference effect similar to the null in $\tilde{\rho}^q_{13}$ in Fig. 7. From Eq. (30), the condition for a null can be stated as $(\rho_{11} - \rho_{22}) = (\rho_{22} - \rho_{33})$. For full resonance and a weak harmonic, the saturated value of the diagonal element can be found from an algebraic solution of the equations in Appendix B and yield the value of Λ_{23} for which a null occurs. For $\rho^e_{11} = 1$, the condition is expressed as $T_2^2\Lambda_{23}^2 = T_2^2\Lambda_{12}^2/2 - 1/4$. From this, $R_\mu = \Lambda_{23}/\Lambda_{12}$. For large Λ_{12}, this yields $R_\mu = 1/\sqrt{2}$ while as $R_\mu \to 0$, $T_2\Lambda_{12} \to 1/\sqrt{2}$. The worst possible case is when $R_\mu = 1/\sqrt{2}$ for which the parametric gain is zero except at low field values in which case the conversion is small. For R_μ values larger than those needed to satisfy the null condition, $\tilde{\rho}^q_{13}$ is negative while for all other values it is positive. The precipitous dip in the conversion for $R_\mu = 0.35$ in Fig. 9 is due to the population interference effect and the phase reversal of $\tilde{\rho}^q_{13}$ which only occurs for $R_\mu < 1/\sqrt{2}$ and which results in the existence of two maxima in the harmonic intensity at two different lengths.

In all other cases investigated, detuning degraded the conversion when the pump Rabi frequencies were less than the detunings. For the opposite case, severe power broadening resulted in a saturatedlike behavior and a large conversion. However, from Figs. 4(b)–4(d), the existence of dispersion on harmonic resonance implies that the large conversion results should be viewed pessimistically because of phase match difficulties.

The effects of temperature in thermally populating the excited states reduce $\tilde{\rho}^q_{13}$, as can be seen in Eq. (31), and hence increase the conversion distance ζ_m. Although this effect was not explored for all possible situations, one example is seen for the case of Fig. 8(a) when $\hbar\Omega_{21} = kT$ for which the conversion is reduced to 53% at $\zeta_m = 11.2$.

V. OTHER PARAMETRIC CASES

The major implications of the last two sections can be extended to the other parametric cases associated with the linkage diagram of Fig. 1(a). For the case of sum and difference frequency generation which involve two input fields, no major difference is expected in the strength of the conversion process provided both fields are strong. The extended media treatment of these cases will, of course, require three coupled Maxwell equations.

The case of resonant parametric oscillation is different in that only one strong input wave exists. Anticipating a maximum parametric interaction on full resonance, let $\vec{\mathcal{E}}_3$ be a strong pump on resonance. The effect of this field is to saturate the population difference $\rho_{11} - \rho_{33}$ and to split $|1\rangle$ and $|3\rangle$ into two symmetric doublets located $\pm|\Lambda_{13}|$ from the "bare" states. Since this creates degenerate laser and Raman gain contributions sensed by $\vec{\mathcal{E}}_2$, the latter may naturally evolve detuned $\pm|\Lambda_{13}|$ from line center. If $\vec{\mathcal{E}}_1$ is to evolve as a parametric field, conservation of energy requires $\Omega_{31} - \omega_3 = 0 = \Omega_{32} - \omega_2 + \Omega_{21} - \omega_1 = \pm|\Lambda_{13}| + \Omega_{21} - \omega_1$ or ω_1 is detuned the opposite amount from Ω_{21} as is ω_2 from Ω_{32}. The two situations are sketched in Fig. 10. The parametric gain, determined by $\tilde{\rho}^b_{12}$, can be found in the limit Λ_{12}, $\Lambda_{23} \to 0$ and is

$$\tilde{\rho}^b_{12} = \frac{\Lambda_{13}\Lambda^*_{23}}{L^b_{12}}\left(\frac{(\rho_{11}-\rho_{33})}{L^b_{13}} + \frac{(\rho_{22}-\rho_{33})}{L^a_{32}}\right)\frac{1}{\left(1 - \dfrac{|\Lambda_{13}|^2}{L^b_{12}L^a_{32}}\right)}, \tag{44}$$

which again shows the possibility of an interference. Taking $\rho_{11} \cong \rho_{33} \cong \rho^e_{11}/2$, $\Omega_{31} - \omega_3 = 0$, and $\Omega_{32} - \omega_2 = \pm|\Lambda_{13}|$, Eq. (44) simplifies to

$$\tilde{\rho}^b_{12} \cong \pm i\rho^e_{11}e^{i\theta_3}\Lambda^*_{23}/4 \ll 1, \tag{45}$$

where $\pm$ refers to the two possible values of ω_1. This may lead to the generation of two frequencies separated by $2|\Lambda_{13}|$ and 180° out of phase; however, this may not be too probable because these two frequencies coincide exactly with the $|1\rangle \to |2\rangle$ absorption doublets. Alternately, if ω_2 and ω_1 evolved exactly on line center, Eq. (44) simplifies to

$$\tilde{\rho}^b_{12} \cong -\frac{\Lambda^*_{23}}{2\Lambda^*_{13}}\rho^e_{11}, \tag{46}$$

which is even smaller than in Eq. (45). This leads us to conclude that resonant parametric oscillation may be observable, but that the overall effect will

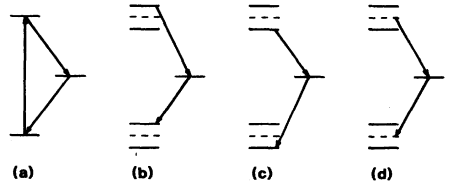

FIG. 10. (a) Linkage diagram for a parametric oscillator. With a strong pump, $\vec{\mathcal{E}}_3$, the upper and lower pump states are split into doublets located $\pm|\Lambda_{13}|$ from the bare states. (b)–(d) The doublets are shown as solid lines while the bare state is a dashed line. The three cases correspond to the three combinations of frequencies ω_1, ω_2 which satisfy the parametric resonances.

be far weaker than parametric effects caused by two input waves.

VI. CONCLUSIONS

In this paper, a semiclassical analysis of three-wave parametric interactions in a three-level system was developed and applied to the case of second-harmonic generation. Within the validity of the rotating wave and adiabatic approximations, the solutions presented for the nonlinear polarizations in terms of saturated diagonal elements were shown to be nonperturbative. The inherent multiphoton nature of the interactions was shown to split the harmonic transition into a multiplet which generally reduced potential absorption of the harmonic.

Numerical solutions of the coupled Maxwell–density-matrix equations indicated the possibility of high conversion, $>50\%$, provided $R_\mu \gtrsim 1$. The origin of the high conversion, which occurs on full resonance, can be traced to a very large nonlinear polarization, low harmonic absorption, and to the fact that the strongly saturating pump decays only linearly due to saturation of the absorption. As in the case of normal second-harmonic generation in transparent media, the initial growth of the harmonic is parabolic in the space coordinate but is in direct contrast in that the conversion distance increases with pumping intensity.

The existence of an interference effect in the weak-field and strong-field limits was noted and has as its origin the fact that the parametric contributions from $|2\rangle$ enters with a sign opposite to those from $|1\rangle$ and $|3\rangle$. This sign difference is due to the sign (phase) of the absorption-emission sequence amplitude of the virtual parametric process associated with $|2\rangle$ as opposed to the absorption-absorption (emission-emission) sequence associated with $|1\rangle$ ($|3\rangle$). The primary effect is to cause a very low parametric gain for certain $R_\mu < 1$ values which also depends on the pumping field intensity.

The highest conversion efficiency occurred for $R_\mu > 2$ for which the pump absorption is reduced. The multiphoton nature of the interaction again became important in that for large R_μ, the pump essentially splits its absorption out of resonance reducing saturation and hence absorption. This most unusual situation yielded the highest conversion efficiency in the shortest distances.

The general requirements for the attainment of high conversion are $R_\alpha \sim 2$, $R_\mu > 2$, and $T_2\Lambda_{12} > 3$ for which a conversion of $>50\%$ will occur at an interaction distance $z_m > 16/\alpha_{12}$ where α_{12} is the line-center Beer's coefficient for the $|1\rangle \rightarrow |2\rangle$ transition. The relative effects of nonequal T_1 and T_2 values were not explored but are anticipated to be small provided $\Lambda_{ij}T_2 > 3$ is maintained.[39] In the solid phase, the transitions may be inhomogeneously broadened, in which case the effects of pump attenuation may be much more severe due to differences in saturation. The inclusion of this latter effect adds sufficient complexity to the problem to warrant a separate study.[40] Aside from this, the large nonlinearity available under resonant, saturated conditions and the reduction of harmonic absorption by level splitting and saturation are both suggestive of further experimental inquiries into the conversion in three-level systems and to the prospects for strong interactions in resonant four-level systems in the form of tripling.

ACKNOWLEDGMENTS

It is a pleasure to acknowledge the valuable contributions of P. D. Coleman, H. K. Chung, S. J. Petuchowski, L. T. Specht, J. R. Tucker, and K. S. Yngvesson. This research was supported by the National Science Foundation (Grant No. ECS 80-03534), the Joint Services Electronics Program (Grant No. N00014-79-0424), and the University of Illinois Industrial Affiliates Program.

APPENDIX A

In this appendix, we compile the nonperturbative solutions for the $\tilde{\rho}^l_{ij}$ amplitudes in terms of complex amplitudes which are multipliers to various combinations of differences in diagonal elements. When deriving a solution from a signal flow graph, the form of the latter terms always groups into population differences associated with individual one-photon transitions.[33] We continue to use this "natural" form for the solution and express a general element as

$$\tilde{\rho}^l_{ij} = A^l_{ij}(\rho_{11}-\rho_{22}) + B^l_{ij}(\rho_{22}-\rho_{33}) + C^l_{ij}(\rho_{33}-\rho_{11}), \tag{A1}$$

where $l = a, b$. Define individual closed path gains as $A = |\Lambda_{23}|^2/L^b_{13}L^b_{12}$, $B = |\Lambda_{13}|^2/L^b_{12}L^a_{32}$, $C = |\Lambda_{12}|^2/L^a_{32}L^a_{31}$, $D = |\Lambda_{23}|^2/L^a_{31}L^a_{21}$, $E = |\Lambda_{13}|^2/L^a_{21}L^b_{23}$, and $F = |\Lambda_{12}|^2/L^b_{23}L^b_{13}$ and a graph determinant as $\Delta = 1 - (A+B+C+D+E+F-2BDF) + (AE+AD+AC+FD+FC+FB+EC+EB+DB) - (ECA+DBF)$.[33] With these, the coefficients are found to be given by

$$A^a_{13} = \frac{\Lambda_{12}\Lambda_{23}}{L^a_{12}L^a_{13}\Delta^*}(1-A-B-F)^*, \tag{A2}$$

$$B^a_{13} = -\frac{\Lambda_{12}\Lambda_{23}}{L^a_{23}L^a_{13}\Delta^*}(1-A-E-F)^*, \tag{A3}$$

$$C^a_{13} = -\frac{\Lambda_{12}\Lambda_{23}}{L^b_{31}L^a_{13}\Delta^*}(E-B)^*, \tag{A4}$$

$$A^b_{13} = -\frac{\Lambda_{13}}{L^a_{21}\Delta}[F(1-C-B)-AC], \tag{A5}$$

$$B^b_{13}=-\frac{\Lambda_{13}}{L^a_{32}\Delta}[A(1-E-D)-DF]\,, \tag{A6}$$

$$C^b_{13}=\frac{\Lambda_{13}}{L^b_{13}\Delta}(1-E-D-C-B+EC+DB+EB)\,, \tag{A7}$$

$$A^a_{12}=-\frac{\Lambda_{12}}{L^a_{12}\Delta^*}(1-C-B-A-F+CA+CF+BF)^*\,, \tag{A8}$$

$$B^a_{12}=\frac{\Lambda_{12}}{L^a_{23}\Delta^*}[D(1-F-A)-AE]^*\,, \tag{A9}$$

$$C^a_{12}=\frac{\Lambda_{12}}{L^b_{31}\Delta^*}[E(1-B-C)-DB]^*\,, \tag{A10}$$

$$A^b_{12}=\frac{\Lambda_{13}\Lambda^*_{23}}{L^a_{21}L^b_{12}\Delta}(F-C)\,, \tag{A11}$$

$$B^b_{12}=\frac{\Lambda_{13}\Lambda^*_{23}}{L^a_{32}L^b_{12}\Delta}(1-D-E-F)\,, \tag{A12}$$

$$C^b_{12}=-\frac{\Lambda_{13}\Lambda^*_{23}}{L^b_{13}L^b_{12}\Delta}(1-F-D-C)\,, \tag{A13}$$

$$A^a_{23}=\frac{\Lambda_{23}}{L^a_{12}\Delta^*}[C(1-F-A)-FB]^*\,, \tag{A14}$$

$$B^a_{23}=-\frac{\Lambda_{23}}{L^a_{23}\Delta^*}(1-A-F-E-D+AE+AD+DF)^* \tag{A15}$$

$$C^a_{23}=\frac{\Lambda_{23}}{L^b_{31}\Delta^*}[B(1-E-D)-EC]^*\,, \tag{A16}$$

$$A^b_{23}=-\frac{\Lambda_{13}\Lambda^*_{12}}{L^a_{21}L^b_{23}\Delta}(1-A-B-C)\,, \tag{A17}$$

$$B^b_{23}=-\frac{\Lambda_{13}\Lambda^*_{12}}{L^a_{32}L^b_{23}\Delta}(A-D)\,, \tag{A18}$$

$$C^b_{23}=\frac{\Lambda_{13}\Lambda^*_{12}}{L^b_{13}L^b_{23}\Delta}(1-D-C-B)\,. \tag{A19}$$

These coefficients are valid for arbitrary field intensity, phase angle θ_i, and detunings to within the validity of the rotating-wave approximation.

APPENDIX B

Given the complex coefficients in Appendix A, the driving terms in the population equations, Eqs. (15)–(17), can be found. For example, for ρ_{11},

$$\begin{aligned}2\,\mathrm{Im}\left(\frac{\rho_{12}\vec{\mu}_{21}\cdot\vec{E}}{\hbar}\right)&\rightarrow 2\,\mathrm{Im}(\tilde{\rho}^a_{12}\Lambda^*_{12}+\tilde{\rho}^b_{12}\Lambda^*_{12}\bar{F})\\&=2\,\mathrm{Im}[\Lambda^*_{12}(A^a_{12}+A^b_{12}\bar{F})(\rho_{11}-\rho_{22})+\Lambda^*_{12}(B^a_{12}+B^b_{12}\bar{F})(\rho_{22}-\rho_{33})+\Lambda^*_{12}(C^a_{12}+C^b_{12}\bar{F})(\rho_{33}-\rho_{11})]\\&=a_{12}(\rho_{11}-\rho_{22})+b_{12}(\rho_{22}-\rho_{33})+c_{12}(\rho_{33}-\rho_{11})\\&=(a_{12}-c_{12})\rho_{11}+(b_{12}-a_{12})\rho_{22}+(c_{12}-b_{12})\rho_{33}\,,\end{aligned}$$

where $\bar{F}$ is the time average of F given in Eq. (21) and a_{ij}, b_{ij}, and c_{ij} are some new constants. The remaining constants follow from Eqs. (19) and (20) and Eqs. (A2)–(A7) and (A14)–(A19). With these constants, Eqs. (15)–(17) are reduced to a set of three coupled algebraic equations which are readily solved. The solutions for ρ_{ii} are then used to construct the polarizations in terms of the coefficients in Appendix A. The only restriction on the solution is that if $0<|\omega_3-\omega_1-\omega_2|<T_1, T_2$, the fields may beat in the medium causing a modulated polarization. This is not accounted for in the formalism since all $\tilde{\rho}^l_{ij}$ were taken as time independent.

A particularly useful limit can be obtained for full resonance, $\tau_{ii}=\tau_{ij}=T_2$, and when $\vec{\delta}_3\rightarrow 0$. Setting $\lambda_1=T_2^2\Lambda_{12}^2$, $\lambda_2=T_2^2\Lambda_{23}^2$, $a=2\lambda_1(1+\lambda_1)/(1+\lambda_1+\lambda_2)$, $b=2\lambda_2(1+\lambda_2)/(1+\lambda_1+\lambda_2)$, $c=2\lambda_1\lambda_2/(1+\lambda_1+\lambda_2)$, and $d=(1+2a-c)(1+2b-c)-(2c-b)(2c-a)$, the saturated diagonal element difference terms are found to be given by

$$(\rho_{11}-\rho_{22})=[(\rho^e_{11}-\rho^e_{22})(1+2b-c)-(\rho^e_{22}-\rho^e_{33})(2c-b)]/d\,, \tag{B1}$$

$$(\rho_{22}-\rho_{33})=[(\rho^e_{22}-\rho^e_{33})(1+2a-c)-(\rho^e_{11}-\rho^e_{22})(2c-a)]/d\,. \tag{B2}$$

[1]P. A. Franken, A. E. Hill, C. W. Peters, and G. Weinreich, Phys. Rev. Lett. 7, 118 (1961).
[2]J. A. Armstrong, N. Bloembergen, J. Ducuing, and P. S. Pershan, Phys. Rev. 127, 1918 (1962).
[3]J. W. Ward, Rev. Mod. Phys. 37, 1 (1965).
[4]T. Mossberg, A. Flusberg, and S. R. Hartman, Opt. Commun. 25, 121 (1978).
[5]R. T. Hodgson, P. P. Sorokin, and J. J. Wynne, Phys. Rev. Lett. 32, 343 (1974).
[6]C. M. Kellington, Phys. Rev. Lett. 9, 57 (1962).
[7]H. G. Andresen, H. Welling, and C. M. Kellington, Phys. Rev. Lett. 11, 361 (1963).

[8]E. U. Shafer, H. Friedburg, H. Kuiper, J. Lipp, and E. Racknagle, Phys. Lett. 6, 21 (1963).
[9]A. V. Voskanyan, D. N. Klyshko, and V. S. Tumanov, Zh. Eksp. Teor. Fiz. 45, 1399 (1963) [Sov. Phys.—JETP 18, 967 (1964)].
[10]K. S. Yngvesson and E. L. Kollberg, Appl. Phys. Lett. 36, 104 (1980).
[11]H. Inaba and T. Hidaka, Nachrichtentechn. Fachber. 35, 667 (1968); H. Inaba and T. Hidaka, Nature (London) 224, 57 (1969).
[12]G. Dathe, K.-H. Steiner, D. Roth, and G. Schollmeier, IEEE J. Quantum Electron. 5, 623 (1969).
[13]Some examples of second-harmonic generation in resonant two-level systems are R. Boscaino, I. Ciccarillo, and M. W. P. Strandberg, Phys. Rev. B 3, 2175 (1971); G. Dathe, D. Roth, G. H. Schollmeier, and K.-H. Steiner, IEEE J. Quantum Electron. 5, 169 (1969).
[14]A. M. Clogston, J. Phys. Chem. Solids 4, 271 (1958).
[15]I. R. Senitzky, in *Quantum Electronics*, edited by C. H. Townes (Columbia University Press, New York, 1960), pp. 212–214.
[16]H. G. Andresen, H. Welling, and K. D. Möller, in *Quantum Electronics, Proceedings of the Third International Congress, Paris*, edited by P. Grivet and N. Bloembergen (Columbia University Press, New York, 1964), pp. 1597–1602.
[17]N. Bloembergen and Y. R. Shen, Phys. Rev. 133, A37 (1964); N. Bloembergen, *Nonlinear Optics* (Benjamin, New York, 1965), Appendix III.
[18]T. Hänsch and P. Toschek, Z. Phys. 236, 373 (1970).
[19]K. -H. Steiner, *Interactions Between Electromagnetic Fields and Matter* (Pergamon, Oxford, 1973), Chap. V.
[20]E. G. Soloviev, A. V. Stantsev, and K. K. Pukhov, Nachrichtentechn. Fachber. 35, 750 (1968).
[21]A. Javan and A. Szöke, Phys. Rev. 137, A536 (1965).
[22]J. E. Bjorkholm and P. F. Liao, Phys. Rev. Lett. 33, 128 (1974).
[23]R. M. Whitley and C. R. Stroud, Jr., Phys. Rev. A 14, 1498 (1976).
[24]C. Cohen-Tannoudji and S. Reynaud, J. Phys. B 10, 2311 (1977).
[25]G. R. Osche, J. Opt. Soc. Am. 68, 1293 (1978).
[26]R. Salomaa and S. Stenholm, Appl. Phys. 17, 309 (1978).
[27]S. H. Autler and C. H. Townes, Phys. Rev. 100, 703 (1955).
[28]R. E. Grove, F. Y. Wu, and S. Ezekiel, Phys. Rev. A 15, 227 (1977).
[29]H. R. Gray and C. R. Stroud, Jr., Opt. Commun. 25, 359 (1978).
[30]S. J. Petuchowski, J. D. Oberstar, and T. A. DeTemple, Phys. Rev. A 20, 529 (1979).
[31]For simplicity, we neglect the Lorentz local field factors which would be needed to treat condensed media. See, for example, R. H. Pantell and H. E. Putoff, *Fundamentals of Quantum Electronics* (Wiley, New York, 1969), Appendix 4.
[32]L. R. Wilcox and W. E. Lamb, Jr., Phys. Rev. 119, 1915 (1960).
[33]H. K. Chung and T. A. DeTemple, Phys. Rev. A 22, 2647 (1980).
[34]T. A. DeTemple, H. K. Chung, and S. J. Petuchowski, Int. J. Infrared Millimeter Waves 1, 27 (1980).
[35]Since the diagonal elements appear as 'inputs' in the graph representation, the solutions are written in a natural form including population differences associated with separate one-photon transitions. They can always be rewritten in terms of separate population differences involving one-, two-, ... photon transitions if desired. See Refs. 30 and 33.
[36]T. A. DeTemple, S. J. Petuchowski, and H. K. Chung, Phys. Rev. A 22, 2636 (1980).
[37]From Ref. 24, the dressed states for this example are located at 0, $\pm\lambda$ relative to the bare state where $\lambda = (\Lambda_{12}^2 + \Lambda_{23}^2)^{1/2}$. Taking all possible differences between two sets of dressed states yields candidate resonances at 0, $\pm\lambda, \pm 2\lambda$ relative to line center. The result in Eq. (27) shows that only two of the five possible transitions are optically allowed.
[38]For example, by manipulating the results in Appendix A, level splittings caused by the strong pump are counteracted by a strong harmonic when $\Lambda_{13}^2 \cong \Lambda_{12}^2 + \Lambda_{23}^2$ on full resonance. When this condition occurs, the $|1\rangle \rightarrow |3\rangle$ absorption multiplet contracts back into a singlet sensed by ω_3 and transitions from these states to $|2\rangle$ start to become split by the harmonic.
[39]The effects of nonequal decay and dephasing rates in a parametric interaction with a strong pump but weak signal and idler fields was considered in A. Jeleński, Electron Technol. (Poland) 3, 127 (1970).
[40]L. A. Bahler (unpublished).